Communications

Sai Sunil Kumar Mallineni, Herbert Behlow, Ramakrishna Podila* and Apparao M. Rao*

A low-cost approach for measuring electrical load currents in triboelectric nanogenerators

https://doi.org/10.1515/ntrev-2017-0178
Received September 12, 2017; accepted October 11, 2017; previously published online November 22, 2017

Abstract: Research into the development of triboelectric nanogenerators (TENGs) has exponentially expanded over the last 5 years with TENGs expected to be a prominent alternative energy-harvesting source in the near future. Notwithstanding the rapid progress in TENG development and their applications, the start-up cost of required research equipment and components remains high for new entrants into the field. A substantial portion of that cost is for the preamplifier, which is needed for measuring the output current of a TENG. Here, an ultra-low-cost device is presented that can measure the TENG output current, which is a crucial parameter in the characterization of TENG electrical performance. This alternative approach is expected to enable research groups in the future to partially offset the initial expense of instrumentation necessary for TENG research, and accelerate the development and applications of TENGs.

Keywords: current preamplifier; low-cost measurement; triboelectric nanogenerator.

1 Introduction

A well-known English proverb, "Necessity is the mother of invention", succinctly affirms the primary motivation for much scientific research in renewable energy. With growing global energy demands, concerted efforts have been expended to improve the efficiency of sustainable energy technologies such as photovoltaics, wind energy, fuel cells, and recently, triboelectric nanogenerators (TENGs) that convert mechanical energy into usable electric power [1–6]. TENG has been demonstrated as a fundamentally new green energy technology, featured as being simple, reliable, cost-effective, as well as highly efficient [7–10]. In its simplest form, a TENG consists of two suitable triboelectric materials appropriately chosen based on their position in triboelectric series [11, 12]. When brought into physical contact, the friction between these materials induces the separation of electrostatic charges at the interface. By suitably engineering the device architecture, these charges can be extracted into an external circuit to perform electrical work. Based on this principle, several modes of TENG operation have been developed, viz. (i) the vertical contact separation mode [13–15], (ii) the in-plane sliding mode [16–19], (iii) the single-electrode mode [20–22], and (iv) the free-standing triboelectric layer mode [23, 24]. The potential of these different configurations of TENGs has been demonstrated, not only as sustainable power sources to harvest energy from water waves [25, 26], wind flow [27, 28], acoustic waves [29], and human walking [30, 31], but also in biomedical monitoring [32, 33], chemical sensing [34, 35], and human-machine interfacing [36]. Irrespective of the design and device architecture of the TENGs for harvesting mechanical energy, TENGs are characterized as having an (i) open-circuit voltage (V_{OC}), (ii) a short-circuit current (I_{SC}), (iii) a power density (i.e. output power per unit area or P), and (iv) capacitor charging (i.e. output current into approximately constant voltage loads). Although the V_{OC}, I_{SC}, and capacitor charging are measured experimentally using laboratory instruments, the power density is a derived quantity ($P = VI$). Typically, a digital oscilloscope is employed for measuring TENG voltages, while a Stanford Research Systems SR570 (http://www.thinksrs.com/) low-noise current preamplifier (LNCP) is widely used for measuring the ultra-low currents delivered by TENG [37–56]. While digital oscilloscopes are readily available in most laboratories, an LNCP is far less commonly available, and often must be purchased. The list price of the SR570 at the time of this writing is $2595 on the thinksrs.com

***Corresponding authors: Ramakrishna Podila,** Clemson Nanomaterials Institute, Department of Physics and Astronomy, Clemson University, Clemson, SC 29634, USA; and Laboratory of Nano-biophysics and COMSET, Clemson University, Clemson, SC 29634, USA, Phone: 864-656-4447, Fax: 864-656-0805, e-mail: rpodila@g.clemson.edu; and **Apparao M. Rao,** Clemson Nanomaterials Institute, Department of Physics and Astronomy, Clemson University, Clemson, SC 29634, USA, Phone: 864-656-4447, Fax: 864-656-0805, e-mail: arao@g.clemson.edu
Sai Sunil Kumar Mallineni and Herbert Behlow: Clemson Nanomaterials Institute, Department of Physics and Astronomy, Clemson University, Clemson, SC 29634, USA

website. Given that LNCPs are also needed for characterization of other energy generation devices such as quantum efficiency of photovoltaic modules in addition to TENGs, the development of simple and inexpensive LNCPs can be helpful to the energy research community.

In this article, we describe a low-cost approach for measuring the electrical currents generated by a TENG. Our method essentially consists of an in-house-assembled current preamplifier comprising a simple current-to-voltage converter circuit, which can be substituted for the SR570 at a fraction (~2%) of the cost.

2 Background – why a current preamplifier?

The output voltage produced by TENGs depends upon such criteria as the triboelectric materials, the device geometry, the applied force and frequency, and the ambient temperature and relative humidity. Although TENG voltages can range from a few millivolts to several thousand volts, TENGs are inherently low-output-current devices, often with values in the range of ~nA to ~μA for a laboratory-scale TENG (approximately few cm^2 area). Moreover, laboratory-scale TENGs deliver maximum output power into resistive loads that are of the order of a few MΩ, implying a similar level of impedance for the TENG itself. The high intrinsic impedance of TENGs complicates voltage or current measurements, because the voltmeter (or oscilloscope) input loads the device, and will typically sink a significant portion of the TENG output current. In other words, because TENGs are low-output-current devices, it is difficult to perform the current measurements with minimal perturbations to the TENG output current.

Of the various approaches for measuring TENG output current, connecting the TENG to a resistive load and measuring the voltage drop across the resistor is the simplest, with Ohm's law providing the current, $I = V/R$. Although theoretically straightforward, several problems prevent its practical application. First, as noted above, the input impedance of the voltmeter (or oscilloscope) is of the same order as the output impedance of the TENG, which places a significant additional load upon the TENG, in parallel to the designated load resistance. Consequently, the TENG output voltage is reduced to some extent, which makes the measurement inaccurate. Attempts to compensate for this by calculating the equivalent load resistance (i.e. the load resistor combined in parallel with the impedance of the voltmeter or scope) are problematic because of the input capacitance of the voltmeter or scope, which is characterized by frequency-dependent impedance.

A further complication of the resistive-voltage-drop method is from a greater interest in determining the output current of a TENG into low-impedance loads (or even into a short-circuit load). According to Ohm's law, the voltage drop is proportional to resistance for a given current. When the load resistance is small compared to the TENG impedance (i.e. ≤1 MΩ), the voltage drop will be small and may be comparable to the signal noise, resulting in excessive uncertainty in the measurement. Moreover, the extreme case of a short-circuit load prevents measurement of the current because the voltage drop is then equal to zero.

3 Circuit description and device performance

To overcome the difficulties mentioned above, an active device [i.e. an operational amplifier (op-amp)] is employed in the measurement circuit. Op-amps are ubiquitous in a wide range of modern electronics applications and readily available at low cost in easy-to-use integrated circuit (IC) packages. To meet our requirements, the Texas Instruments LMC6001 Ultra-Low Input Current Amplifier IC was selected as the heart of our LNCP (cf. Figure 1D). With a typical input current (an ideal op-amp has zero input current) of <25 fA, the LMC6001 can measure the current down to the ~pA range, which is several orders of magnitude smaller than the typical TENG output current. In addition to the peak value of current generated by the TENG, an accurate acquisition of the output current waveform, which may contain high-frequency components (i.e. $f > 10$ kHz), is also important. An amplifier with a sufficient bandwidth is necessary for acquiring these dynamic signals, and the LMC6001 with its 1.6 V/μs slew rate is easily capable of meeting this requirement.

As shown in Figure 1D, the LMC6001 op-amp is configured as an inverting current-to-voltage converter consisting of a 10 kΩ feedback resistor from the output to the inverting input, resulting in a sensitivity of 10 mV/μA (or equivalently 100 μA/V). The circuit operation is best explained by an example in which we assume an input current of 1 μA generated by a TENG enters the op-amp. The op-amp output produces an equal and opposite current via the feedback resistor to the inverting input, resulting in 0 V at the inverting input. As an ideal op-amp has infinite input impedance, zero or no current enters the op-amp, and the feedback current exactly balances the input current to be measured. Although not infinite, the input impedance in an actual op-amp is often large enough for the input current to be insignificant (the LMC6001 has an input impedance of ~10^{12} Ω). The 1 μA feedback current flowing through the 10 kΩ resistor

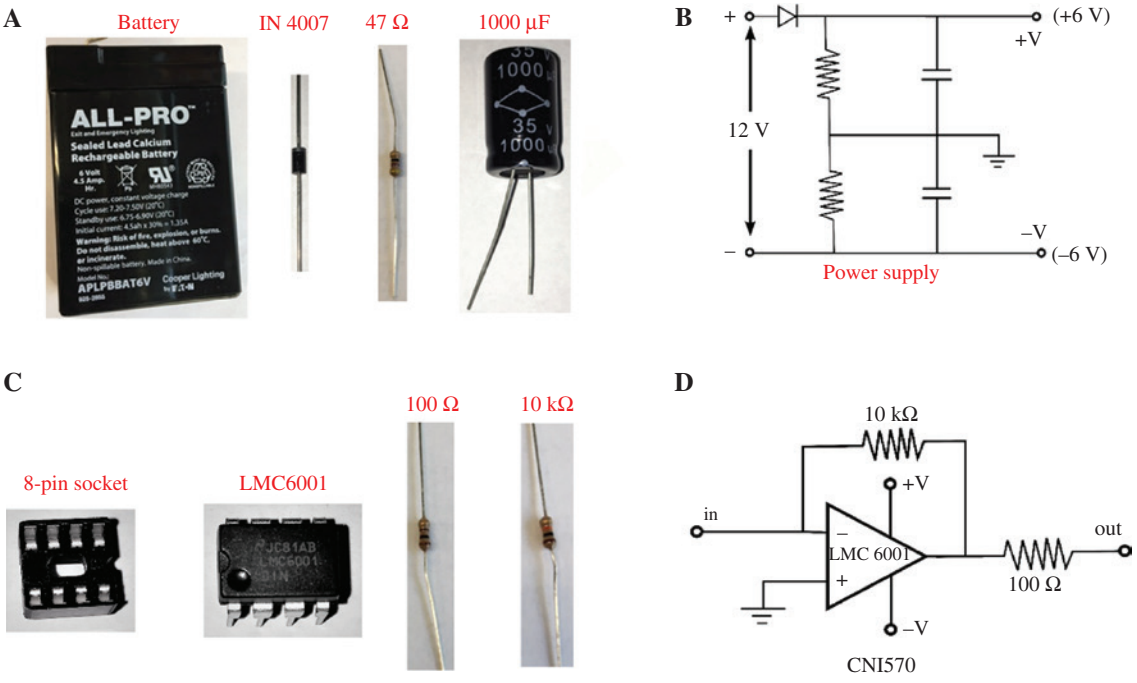

Figure 1: (A) Required components for power supply. (B) Schematic of CNI570 power supply. (C) Required components for assembly of CNI570. (D) Circuit diagram of CNI570.

results in a voltage of 10 mV appearing at the amplifier output, and accordingly, the sensitivity is 10 mV/µA. Other values of feedback resistor may be substituted to vary the sensitivity as required for any particular experiment; for example, 100 kΩ will result in a sensitivity of 100 mV/µA, and 1 kΩ a sensitivity of 1 mV/µA. It should be noted that the inverting configuration of the amplifier results in a negative output voltage when the input current is positive. This inversion is generally of no consequence, as the amplitude of the output voltage is of primary interest. However, if one wishes to preserve the sign of the signal, it is a trivial matter to add a second op-amp (such as a Texas Instruments TL082, which has sufficient bandwidth, and is inexpensive) configured as a unity-gain inverting amplifier to invert the signal from the output of the LMC6001.

4 Experimental: TENG test device and CNI570

To evaluate our in-house-assembled current preamplifier and compare its performance to the SR570, we used a reference test signal provided by a TENG fabricated from off-the-shelf materials [15]. Briefly, our TENG test device is comprised of top and bottom triboelectric layers configured in a vertical contact separation mode: the top TENG triboelectric layer was an indium tin oxide (ITO)-coated polyethylene terephthalate (PET) film, and the bottom triboelectric layer was a polyimide (KAPTON™) film attached to the ITO surface of an ITO-coated PET film. The top and bottom triboelectric sheets were separated by insulating glass spacers that provided an air gap of ~1 mm. A custom-built pushing actuator was used to exert a force of ~35 N at a frequency of ~2.0 Hz, and the TENG output voltage was measured using a Yokogawa DL9710L digital oscilloscope. The V_{OC} of our TENG test device was ~500 V. All tests were performed in ambient conditions (20°C and 43% relative humidity).

To measure the output current of our TENG test device, we built a prototype of the simple current preamplifier (described above) at the Clemson Nanomaterials Institute or CNI (hereafter referred to as the CNI570), which was assembled in-house using inexpensive, readily available components, viz. resistors, capacitors, and an op-amp IC. The circuit consists of two sections: (i) a voltage divider, which allows a single 12-V battery to function as a bipolar power supply (i.e. +6V, −6V, and ground), and (ii) an op-amp-based current-to-voltage converter. The components of the voltage divider circuit and its schematic are shown in Figure 1A and B, respectively. Similarly, the components and the schematic of the current-to-voltage converter circuit are shown in Figure 1C and D, respectively. The approximate cost for the components of the CNI570 (including the voltage divider components as per above)

Table 1: Cost estimates of components required for the fabrication of CNI570.

Unit	Qty	Estimate price
Rechargeable battery (6 V)	2	$20 × 2 = $40
IN 4007	1	$0.16
47 Ω Resistor	2	$0.088 × 2 = $0.176
1000 µF capacitor	2	$0.8 × 2 = $1.6
8-pin socket	1	$0.10
10 kΩ Resistor	1	$0.088
100 Ω Resistor	1	$0.088
LMC6001 ultra-low input current amplifier	1	$17
	Total = 11	~ Total = $60

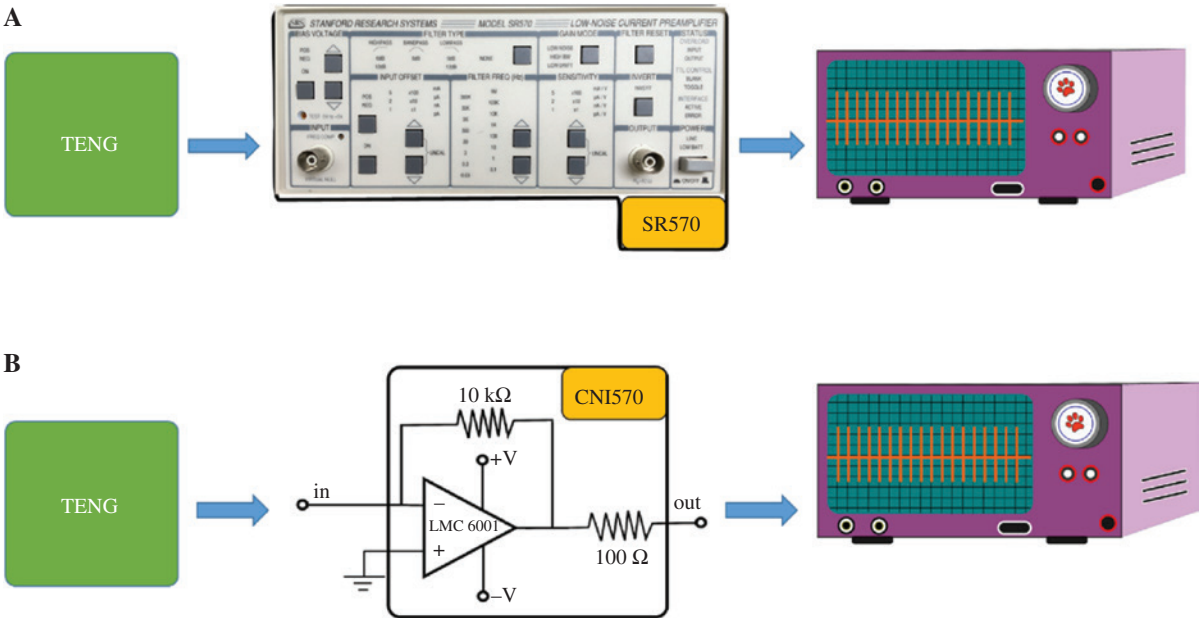

Figure 2: Schematic illustration to measure electrical currents generated by TENG device using (A) SR570 and (B) CNI570.

is itemized in Table 1, which based on the present market price is ~$60.

To assess the performance and accuracy of the CNI570, we measured the TENG output current into several load resistances, viz. 1, 2.2, 4.8 and 9.8 MΩ. As shown in Figure 2A and B, the output current from the TENG was fed alternately into the SR570 and CNI570. The sensitivity of 10 µA/V was selected on the SR570, and the output signals of the SR570 and CNI570 were acquired with a digital oscilloscope.

5 Results and discussion

5.1 Peak current amplitude

The current measurements of the CNI570 were compared with the state-of-the-art SR570, the results of which are shown in Figure 3A–D. The as-measured peak current amplitudes are summarized in Table 2. The CNI570-measured current amplitudes, as shown in Figure 3 and Table 2, are essentially identical to those measured by the SR570 with a mere difference of ~5%. Much of this difference is attributed to the 5% tolerance of the 10 kΩ feedback resistor that was used. To reduce the disparity (and increase accuracy), a 1% precision resistor may be easily substituted for the 5% tolerance general-purpose resistor.

5.2 Theoretical and experimental bandwidth

In addition to the peak current values, the importance of the current waveform from the TENG requires considering the bandwidth (i.e. frequency response) of the current preamplifier. The bandwidth of the SR570 is specified

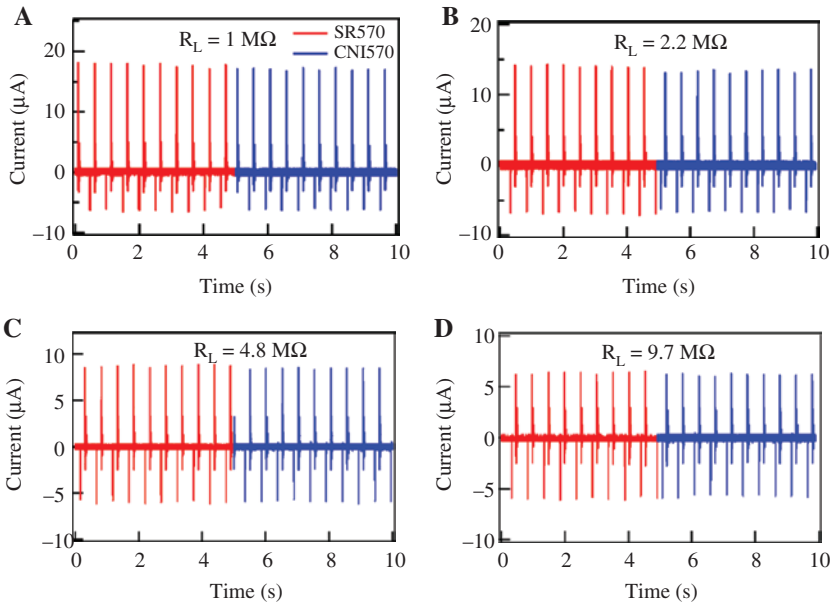

Figure 3: (A–D) Comparison of output currents generated by TENG device through various load resistances measured using SR570 (red) and CNI570 (blue).

Table 2: Comparison of electrical currents measured by the SR570 and CNI570 through different load resistances.

Load resistance across TENG (MΩ)	Peak current measured by SR570 (μA)	Peak current measured by CNI570 (μA)	% Difference
1	18.2	17.3	5.07
2.2	14.3	13.6	5.01
4.8	8.9	8.5	4.59
9.8	6.1	6.3	3.23

As seen from the table, the currents measured by the CNI570 are slightly lower (~5%) compared to those measured by the SR570. This small percentage difference is attributed to the tolerances of the resistors used in the CNI570 (cf. Figure 1D).

as 1 MHz or more specifically as a slew rate limit of 2 V_{pp} at 1 MHz at its output. This specification is equivalent to the highest frequency signal of the SR570 expressed as $V=\sin(2\pi ft)$, where $f=1$ MHz. The slew rate is the maximum rate of change $(dV/dt)_{max}$ of the signal, which is given by the maximum value of $dV/dt=2\pi f\cos(2\pi ft)$. Thus, $(dV/dt)_{max}=2\pi f$ V/s = 6.28 V/μs. The specifications of the LMC6001 op-amp indicate a slew rate of 1.6 V/μs. Thus, the bandwidth of the CNI570 is roughly one-fourth of that of the SR570. In other words, for a 2 V_{pp} output signal from the CNI570, the upper limit of the frequency should be 250 kHz. In a situation where more bandwidth is needed, an n-fold smaller feedback resistor may be used to decrease the sensitivity of the CNI570. The output voltage is thus reduced n-fold (assuming the input current is unchanged) at the expense of a lower signal-to-noise ratio (i.e. the amplifier noise remains unchanged with a signal output that is n-fold lower). To increase the amplitude, the optional inverting op-amp (mentioned previously) may be configured for n-fold gain to restore the amplitude to its original value. The result would be an n-fold increase in bandwidth over 250 kHz. Indeed, a similar two-stage amplifier scheme is how the SR570 controls its overall gain. Accordingly, it is fair to say that the CNI570 is more or less comparable in bandwidth to the SR570.

In the bandwidth measurements, an inherent limitation is the maximum frequency contained in the output waveforms produced by the TENG. The bandwidth of the CNI570 and SR570 was characterized by carefully inspecting the acquired output current waveforms of the TENG in its pressing and releasing pulses (Figure 4). The releasing and pressing waveforms measured by the CNI570 and SR570 are shown in Figure 5A–D. The waveforms were virtually indistinguishable, and the maximum positive and negative dI/dt (slew rate) of the pressing and releasing pulses were 7.5×10^4 and 7.5×10^3 μA/s, respectively. Dividing by the 100 μA/V sensitivity of the CNI570 gives 750 V/s and 75 V/s for the pressing and releasing waveforms, respectively, which are several orders of magnitude smaller than the 1.6×10^6 V/s specification of the LMC6001. Conversely, to convert the voltage slew rate to current slew rate, the product of the voltage slew rate is taken with the sensitivity in μA/V, i.e. $(dI/dt)_{max}=(1.6\times10^6$ V/s) (100 μA/V) $=1.6\times10^8$ μA/s. The maximum dI/dt from the TENG (which occurs under a short-circuit load) is far

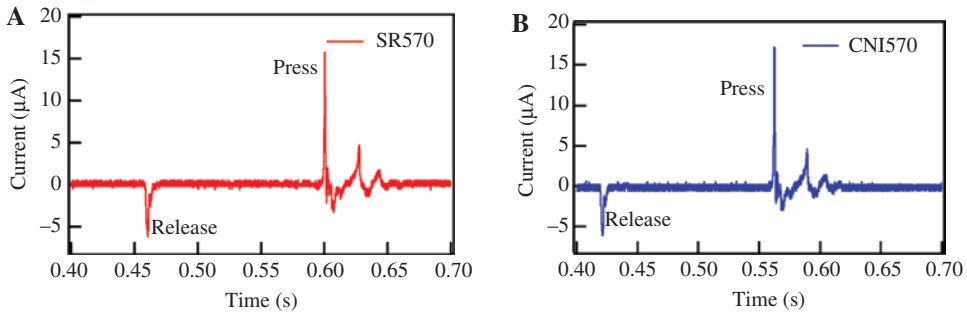

Figure 4: A zoomed-in view of output current generated by TENG during a single cycle of operation (press and release) measured using (A) SR570 and (B) CNI570.

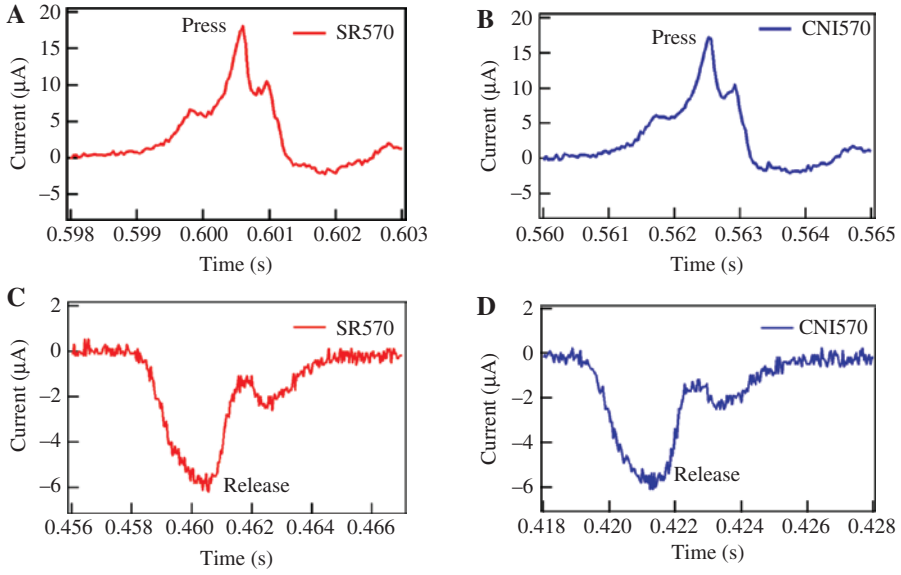

Figure 5: Comparison of electrical currents generated by TENG during pressing and release cycle of its operation. Pressing cycle peaks measured by (A) SR570 and (B) CNI570. Release cycle peaks measured by (C) SR570 and (D) CNI570. As seen in A–D, CNI570 is similar in performance to SR570.

lower than the theoretical maximum capability of the amplifier. Thus, it is no surprise that both the CNI570 and the SR570 are able to measure the full bandwidth of the time-dependent current signal produced by the TENG.

6 Conclusion

The performance of the CNI570 is similar to that of the expensive SR570 instrumentation that is presently in use within the TENG community. As detailed and demonstrated in this study, the CNI570 is a simple and cost-effective precision current preamplifier for measuring low-amplitude, dynamic current signals generated by TENGs. Rather than merely limited to TENGs, the CNI570 could extend to research in photovoltaics, piezoelectric generators, thermoelectric generators, or any other context where a small current from a high-impedance source is measured.

Acknowledgments: R.P. and A.M.R. are thankful to Watt Family Innovation Center (2301812) for the financial support. R.P. also thanks Clemson University (X-1460320) for the start-up funds.

References

[1] Kamat PV. Meeting the clean energy demand: nanostructure architectures for solar energy conversion. *J. Phys. Chem. C.* 2007, 111, 2834–2860.

[2] Ginley D, Green MA, Collins R. Solar energy conversion toward 1 Terawatt. *MRS Bull.* 2008, 33, 355–364.
[3] Pena R, Clare JC, Asher GM. Doubly fed induction generator using back-to-back PWM converters and its application to variable-speed wind-energy generation. *IEE Proc. – Electr. Power Appl.* 1996, 143, 231.
[4] Wright PD. Beyond NIMBYism: towards an integrated framework for understanding public perceptions of wind energy. *Wind Energy* 2005, 8, 125–139.
[5] Fan FR, Tian ZQ, Wang ZL. Flexible triboelectric generator. *Nano Energy* 2012, 1, 328–334.
[6] Wang ZL, Chen J, Lin L. Progress in triboelectric nanogenerators as a new energy technology and self-powered sensors. *Energy Environ. Sci.* 2015, 8, 2250–2282.
[7] Zhu G, Chen J, Zhang T, Jing Q, Wang ZL. Radial-arrayed rotary electrification for high performance triboelectric generator. *Nat. Commun.* 2014, 5, 3426.
[8] Zhu G, Zhou YS, Bai P, Meng XS, Jing Q, Chen J, Wang ZL. A shape-adaptive thin-film-based approach for 50% high-efficiency energy generation through micro-grating sliding electrification. *Adv. Mater.* 2014, 26, 3788–3796.
[9] Zhu G, Peng B, Chen J, Jing Q, Wang ZL. Triboelectric nanogenerators as a new energy technology: from fundamentals, devices, to applications. *Nano Energy* 2014, 14, 126–138.
[10] Zheng L, Cheng G, Chen J, Lin L, Wang J, Liu Y, Li H, Wang ZL. A hybridized power panel to simultaneously generate electricity from sunlight, raindrops, and wind around the clock. *Adv. Energy Mater.* 2015, 5, 1501152.
[11] Diaz AF, Felix-Navarro RM. A semi-quantitative tribo-electric series for polymeric materials: the influence of chemical structure and properties. *J. Electrostat.* 2004, 62, 277–290.
[12] Park CH, Park JK, Jeon HS, Chun BC. Triboelectric series and charging properties of plastics using the designed vertical-reciprocation charger. *J. Electrostat.* 2008, 66, 578–583.
[13] Chen J, Zhu G, Yang W, Jing Q, Bai P, Yang Y, Hou TC, Wang ZL. Harmonic-resonator-based triboelectric nanogenerator as a sustainable power source and a self-powered active vibration sensor. *Adv. Mater.* 2013, 25, 6094–6099.
[14] Yang W, Chen J, Jing Q, Yang J, Wen X, Su Y, Zhu G, Bai P, Wang ZL. 3D stack integrated triboelectric nanogenerator for harvesting vibration energy. *Adv. Funct. Mater.* 2014, 24, 4090–4096.
[15] Mallineni SSK, Behlow H, Dong Y, Bhattacharya S, Rao AM, Podila R. Facile and robust triboelectric nanogenerators assembled using off-the-shelf materials. *Nano Energy* 2017, 35, 263–270.
[16] Zhu G, Chen J, Liu Y, Bai P, Zhou YS, Jing Q, Pan C, Wang ZL. Linear-grating triboelectric generator based on sliding electrification. *Nano Lett.* 2013, 13, 2282–2289.
[17] Bai P, Zhu G, Liu Y, Chen J, Jing Q, Yang Q, Ma J, Zhang G, Wang ZL. Cylindrical rotating triboelectric nanogenerator. *ACS Nano* 2013, 7, 6361–6366.
[18] Jing Q, Zhu G, Bai P, Xie Y, Chen J, Han RPS, Wang ZL. Case-encapsulated triboelectric nanogenerator for harvesting energy from reciprocating sliding motion. *ACS Nano* 2014, 8, 3836–3842.
[19] Kuang SY, Chen J, Cheng XB, Zhu G, Wang ZL. Two-dimensional rotary triboelectric nanogenerator as a portable and wearable power source for electronics. *Nano Energy* 2015, 17, 10–16.
[20] Yang Y, Zhang H, Lin ZH, Zhou YS, Jing Q, Su Y, Yang J, Chen J, Hu C, Wang ZL. Human skin based triboelectric nanogenerators for harvesting biomechanical energy and as self-powered active tactile sensor system. *ACS Nano* 2013, 7, 9213–9222.
[21] Yang Y, Zhang H, Chen J, Jing Q, Zhou YS, Wen X, Wang ZL. Single-electrode-based sliding triboelectric nanogenerator for self-powered displacement vector sensor system. *ACS Nano* 2013, 7, 7342–7351.
[22] Su Y, Zhu G, Yang W, Yang J, Chen J, Jing Q, Wu Z, Jiang Y, Wang ZL. Triboelectric sensor for self-powered tracking of object motion inside tubing. *ACS Nano* 2014, 8, 3843–3850.
[23] Wang S, Xie Y, Niu S, Lin L, Wang ZL. Freestanding triboelectric-layer-based nanogenerators for harvesting energy from a moving object or human motion in contact and non-contact modes. *Adv. Mater.* 2014, 26, 2818–2824.
[24] Guo H, Chen J, Yeh MH, Fan X, Wen Z, Li Z, Hu C, Wang ZL. An ultrarobust high-performance triboelectric nanogenerator based on charge replenishment. *ACS Nano* 2015, 9, 5577–5584.
[25] Zhu G, Su Y, Bai P, Chen J, Jing Q, Yang W, Wang ZL. Harvesting water wave energy by asymmetric screening of electrostatic charges on a nanostructured hydrophobic thin-film surface. *ACS Nano* 2014, 8, 6031–6037.
[26] Li X, Tao J, Zhu J, Pan C. A nanowire based triboelectric nanogenerator for harvesting water wave energy and its applications. *APL Mater.* 2017, 5, 074104.
[27] Zhang L, Zhang B, Chen J, Jin L, Deng W, Tang J, Zhang H, Pan H, Zhu M, Yang W, Wang ZL. Lawn structured triboelectric nanogenerators for scavenging sweeping wind energy on rooftops. *Adv. Mater.* 2016, 28, 1650–1656.
[28] Bae J, Lee J, Kim S, Ha J, Lee BS, Park Y, Choong C, Kim JB, Wang ZL, Kim HY, Park JJ, Chung UI. Flutter-driven triboelectrification for harvesting wind energy. *Nat. Commun.* 2014, 5, 4929.
[29] Yang J, Chen J, Liu Y, Yang W, Su Y, Wang ZL. Triboelectrification-based organic film nanogenerator for acoustic energy harvesting and self-powered active acoustic sensing. *ACS Nano* 2014, 8, 2649–2657.
[30] Bai P, Zhu G, Lin ZH, Jing Q, Chen J, Zhang G, Ma J, Wang ZL. Integrated multilayered triboelectric nanogenerator for harvesting biomechanical energy from human motions. *ACS Nano* 2013, 7, 3713–3719.
[31] Hou TC, Yang Y, Zhang H, Chen J, Chen LJ, Wang ZL. Triboelectric nanogenerator built inside shoe insole for harvesting walking energy. *Nano Energy* 2013, 2, 856–862.
[32] Yang J, Chen J, Su Y, Jing Q, Li Z, Yi F, Wen X, Wang Z, Wang ZL. Eardrum-inspired active sensors for self-powered cardiovascular system characterization and throat-attached anti-interference voice recognition. *Adv. Mater.* 2015, 27, 1316–1326.
[33] Lin Z, Chen J, Li X, Zhou Z, Meng K, Wei W, Yang J, Wang ZL. Triboelectric nanogenerator enabled body sensor network for self-powered human heart-rate monitoring. *ACS Nano* 2017, 11, 8830–8837.
[34] Li Z, Chen J, Zhou J, Zheng L, Pradel KC, Fan X, Guo H, Wen Z, Yeh MH, Yu C, Wang ZL. High-efficiency ramie fiber degumming and self-powered degumming wastewater treatment using triboelectric nanogenerator. *Nano Energy* 2016, 22, 548–557.
[35] Chen S, Wang N, Ma L, Li T, Willander M, Jie Y, Cao X, Wang ZL. Triboelectric nanogenerator for sustainable wastewater treatment via a self-powered electrochemical process. *Adv. Energy Mater.* 2016, 6, 1501778.
[36] Yang W, Chen J, Wen X, Jing Q, Yang J, Su Y, Zhu G, Wu W, Wang ZL. Triboelectrification based motion sensor for human-machine interfacing. *ACS Appl. Mater. Interfaces* 2014, 6, 7479–7484.

[37] Chandrashekar BN, Deng B, Smitha AS, Chen Y, Tan C, Zhang H, Peng H, Liu Z. Roll-to-roll green transfer of CVD graphene onto plastic for a transparent and flexible triboelectric nanogenerator. *Adv. Mater.* 2015, 27, 5210–5216.
[38] Mao Y, Geng D, Liang E, Wang X. Single-electrode triboelectric nanogenerator for scavenging friction energy from rolling tires. *Nano Energy* 2015, 15, 227–234.
[39] Liang Q, Yan X, Liao X, Zhang Y. Integrated multi-unit transparent triboelectric nanogenerator harvesting rain power for driving electronics. *Nano Energy* 2016, 25,18–25.
[40] Choi D, Wan D, Yoo D, Je K. Nano energy spontaneous occurrence of liquid-solid contact electrification in nature: toward a robust triboelectric nanogenerator inspired by the natural lotus leaf. *Nano Energy* 2017, 36, 250–259.
[41] Jung W, Kang M, Moon HG, Baek S, Yoon S, Wang Z, Kim S, Kang C. High output piezo/triboelectric hybrid generator. *Sci. Rep.* 2015, 5, 9309.
[42] Kim D, Jeon S, Young J, Seol M, Ouk S, Choi Y. High-performance nanopattern triboelectric generator by block copolymer lithography. *Nano Energy* 2015, 12, 331–338.
[43] Kanik M, Marcali M, Yunusa M, Elbuken C. Continuous triboelectric power harvesting and biochemical sensing inside poly(vinylidene fluoride) hollow fibers using microfluidic droplet generation. *Adv. Mater. Technol.* 2016, 1, 1600190.
[44] Gao X, Huang L, Wang B, Xu D, Zhong J, Hu Z, Zhang L, Zhou J. Natural materials assembled, biodegradable, and transparent paper-based electret nanogenerator. *ACS Appl. Mater. Interfaces* 2016, 8, 35587–35592.
[45] Jang D, Kim Y, Yun T, Koh K, Jeong U, Cho J. Force-assembled triboelectric nanogenerator with high-humidity-resistant electricity generation using hierarchical surface morphology. *Nano Energy* 2016, 20, 283–293.
[46] Zhang L, Jin L, Zhang B, Deng W, Pan H, Tang J, Zhu M, Yang W. Multifunctional triboelectric nanogenerator based on porous micro-nickel foam to harvest mechanical energy. *Nano Energy* 2015, 16, 516–523.
[47] Huang L, Bai G, Wong M, Yang Z, Xu W, Hao J. Magnetic-assisted noncontact triboelectric nanogenerator converting mechanical energy into electricity and light emissions. *Adv. Mater.* 2016, 28, 2744–2751.
[48] Zhao K, Qin Q, Wang H, Yang Y, Yan J, Jiang X. Antibacterial triboelectric membrane-based highly-efficient self-charging supercapacitors. *Nano Energy* 2017, 36, 30–37.
[49] Yong Y, Chung J, Choi D, Jung D, Cho M. Highly reliable wind-rolling triboelectric nanogenerator operating in a wide wind speed range. *Sci. Rep.* 2016, 6, 33977.
[50] Wang M, Li W, You C, Wang Q, Zeng X, Chen M. Triboelectric nanogenerator based on 317L stainless steel and ethyl cellulose for biomedical applications. *RSC Adv.* 2017, 7, 6772–6779.
[51] Dhakar L, Gudla S, Shan X, Wang Z, Eng F, Tay H, Heng C, Lee C. Large scale triboelectric nanogenerator and self-powered pressure sensor array using low cost roll-to-roll UV embossing. *Sci. Rep.* 2016, 6, 22253.
[52] Chen X, Han M, Chen H, Cheng X, Song Y, Su Z, Jiang Y, Zhang H. A wave-shaped hybrid piezoelectric and triboelectric nanogenerator based on P(VDF-TrFE) nanofibers. *Nanoscale* 2017, 9, 1263-1270.
[53] Xia X, Chen J, Guo H, Liu G, Wei D, Xi Y, Wang X. Embedding variable micro-capacitors in polydimethylsiloxane for enhancing output power of triboelectric nanogenerator. *Nano Res.* 2017, 10, 320–330.
[54] Kim DY, Kim HS, Jung JH. Ar plasma treated polytetrafluoroethylene films for a highly efficient triboelectric generator. *J. Korean Phys. Soc.* 2016, 69, 1720–1723.
[55] Shin SH, Kwon YH, Kim YH, Jung JY, Lee MH, Nah J. Triboelectric charging sequence induced by surface functionalization as a method to fabricate high performance triboelectric generators. *ACS Nano* 2015, 9, 4621–4627.
[56] Huang T, Lu M, Yu H, Zhang Q, Wang H, Zhu M. Enhanced power output of a triboelectric nanogenerator composed of electrospun nanofiber mats doped with graphene oxide. *Sci. Rep.* 2015, 5, 13942.